NASA Technical Memorandum 83016

Comparison of Visualized Turbine Endwall Secondary Flows and Measured Heat Transfer Patterns

Raymond E. Gaugler and Louis M. Russell
Lewis Research Center
Cleveland, Ohio

Prepared for the
Twenty-eighth Annual International Gas Turbine Conference
sponsored by the American Society of Mechanical Engineers
Phoenix, Arizona, March 27-31, 1983

NASA

COMPARISON OF VISUALIZED TURBINE ENDWALL SECONDARY FLOWS AND MEASURED HEAT TRANSFER PATTERNS

Raymond E. Gaugler* and Louis M. Russell+

National Aeronautics and Space Administration
Lewis Research Center
Cleveland, Ohio

E-1450

ABSTRACT

Various flow visualization techniques were used to define the secondary flows near the endwall in a large scale turbine vane cascade. The cascade was scaled up from one used to generate endwall heat transfer data under a joint NASA-USAF contract. A comparison of the visualized flow patterns and the measured Stanton number distributions was made for cases where the inlet Reynolds number and exit Mach number were matched. Flows were visualized by using neutrally buoyant helium-filled soap bubbles, by using smoke from oil soaked cigars, and by a new technique using permanent marker pen ink dots and synthetic wintergreen oil. For the first time, details of the horseshoe vortex and secondary flows can be directly compared with heat transfer distributions. Near the cascade entrance there is an obvious correlation between the two sets of data, but well into the passage the effect of secondary flow is not as obvious.

INTRODUCTION

In order to design efficient cooling configurations for the endwall surfaces between the vanes in a gas turbine, a detailed description of the heat transfer from the hot gas is required. However, the convective heat flux distribution on the endwall is highly nonuniform as the result of the complex secondary flows present. The mainstream flow is subjected to turning and acceleration as it passes between the vanes, producing pressure gradients across the flow passage. As the endwall inlet boundary layer approaches the row of vanes it is strongly influenced by these pressure gradients. A horseshoe vortex results from the endwall inlet boundary layer interacting with the blunt leading edge of a vane. The boundary layer rolls up into a vortex near the stagnation point. The vortex then wraps around the vane leading edge and is convected downstream. The leg of the vortex on the suction side of the passage stays close to the vane as it is swept downstream, but the pressure side leg is driven across the passage by the pressure difference, becoming part of the passage vortex. The passage vortex results from the boundary layer within the passage being driven across the passage by the pressure gradients and rolling up when it encounters the suction surface of the vane.

Aerodynamic investigations of the secondary flow patterns have been the object of flow visualization studies for some time. Using smoke, Herzig, et al (1) observed the roll-up of the endwall boundary layer into a passage vortex. They showed very clearly that the deflection of the boundary layer flow from pressure side to suction side varies strongly with distance from the endwall, with the fluid nearer the wall being affected the most. However, due to the relatively sharp leading edge on their vane, they did not observe the horseshoe vortex. Langston, et al (2), and Langston (3) reported detailed aerodynamic measurements in a large-scale turbine rotor cascade, including endwall flow visualization and smoke addition to the boundary layer. They observed the streamlines on the endwall associated with the leading edge horseshoe vortex, and noted that all of the smoke introduced into the endwall inlet boundary layer ended up in the passage vortex. Marchal and Sieverding (4) used smoke and a laser light sheet to visualize a cross section normal to the flow near the leading edge for both a turbine rotor cascade and a turbine stator cascade. With this technique, they obtained a view of the flow pattern in a plane at an instant in time, but did not show the spatial development of the vortex. They did note that the location of the horseshoe vortex core at the cascade exit moved from about midpassage for the stator to close to the suction surface for the rotor. Gaugler and Russell (5) presented flow visualization studies of the horseshoe vortex by photographing neutrally buoyant helium-filled soap bubbles in the vortex. This allowed the path followed by a single element of fluid to be followed as it was entrained in the vortex.

In addition to the visualization studies of the secondary flow patterns, a number of studies have been reported where the heat transfer to a turbine endwall

*Aerospace engineer; member, ASME.
+Aerospace engineer.

was investigated. Blair (6) simulated the passage between two vanes on a large scale and found the endwall heat transfer to be strongly influenced by the existence of the passage vortex near the vane suction surface-endwall corner, particularly in the trailing edge region. He also tested passages with both rounded and sharp leading edges to isolate the effect of the leading edge horseshoe vortex on the endwall heat transfer and found significant variations near the leading edge.

Graziani et al (7) studied the endwall and blade surface heat transfer in a large scale cascade of blades and observed that passage secondary flows greatly influenced the heat transfer. They noted that the endwall inlet boundary layer thickness also had a significant effect on the endwall heat transfer, particularly near the vane leading edge where the horseshoe vortex manifests itself most strongly.

Georgiou et al (8) conducted endwall heat transfer tests in a facility that permitted simulation of turbine Mach number, Reynolds number, and temperature ratio. They concluded that changes in the inlet boundary layer thickness only influenced the heat transfer in the vicinity of the leading edge.

The most complete set of endwall heat transfer data currently available has been reported by Hylton et al (9). Under joint NASA-U.S. Air Force sponsorship, measurements were made of endwall Stanton numbers over a range of conditions that included typical engine operating conditions. The results of that work have been summarized by York et al (10).

In this secondary flow visualization study, the cascade used was scaled directly from that used by Hylton et al (9) for endwall heat transfer. Reynolds number and Mach number in the flow visualization cascade matched selected run conditions in (9). For the first time, details of the horseshoe vortex and secondary flows were directly compared with heat transfer distributions. Flows were visualized by using neutrally buoyant helium-filled soap bubbles, by using smoke from oil soaked cigars, and by a new technique, developed by Langston and Boyle (11), using permanent marker pen ink dots and synthetic wintergreen oil. Direct comparisons were made between endwall contour plots of Stanton number and the paths taken by bubbles in the horsesnoe vortex. The surface flow visualization features were also compared with the heat transfer data.

APPARATUS AND PROCEDURE

Cascade

The facility used in this study was the same as that used by Gaugler and Russell (5) with the exception of the test vanes. For this work, the six vanes used were scaled up by a factor of 1.9 from the profile used by Hylton et al (9) for the endwall heat transfer tests. The pertinent cascade parameters were: Axial chord, 9.75 cm (3.84 in); chord/axial chord, 1.78; pitch/axial chord, 1.29; aspect ratio (span/axial chord), 1.56; air inlet angle, 0° (axial); air exit angle, 72°.

Air flow through the cascade was drawn in from an atmospheric inlet and exhausted to the laboratory central exhaust system. The wind tunnel built to hold the cascade is shown schematically in Fig. 1. The inlet nozzle was designed for constant acceleration of the flow through it, as described in (12). At the end of the inlet nozzle the flow enters a duct, 68.6-cm (27-in) wide by 15.2-cm (6-in) high by 152.4-cm (60-in) long. This duct was long enough to ensure a turbulent endwall boundary layer, which was confirmed by profile measurement.

The tunnel boundary layer profile was measured at a point 21.6 cm (8.5 in) upstream of the vanes. The cascade of six vanes was located at the end of the inlet duct. The end vanes had adjustable tailboards to assure periodicity of the flow through the cascade. One of the vanes in the center of the cascade was instrumented with static pressure taps around the vane at midspan. The cascade inlet Reynolds number, based on true chord, ranged from 0.7×10^5 to 3.2×10^5 for the tests described. From the cascade, the flow was ducted to the laboratory central exhaust system. The vanes were fabricated from wood and painted black to provide contrast in the pictures. The rest of the cascade was built of clear acrylic plastic with the bottom endwall painted black.

Flow visualization techniques

There is a slot in the endwall located about 21 cm (8.25 in) upstream of the vane leading edges, shown in Fig. 1. The helium bubbles used for flow visualization are injected into the boundary layer from a plenum beneath this slot. The bubble generating system is described in detail by Hale et al (13), and its use in this facility is described in (5). The desired bubble size and neutral buoyancy are achieved by proper adjustment of air, bubble solution, and helium flow rates. As many as 300 bubbles per second are formed in this device. For these tests the bubble diameter was about 1.5 mm (0.06 in). The bubble generator head was placed through a grommet in the wall of the plenum beneath the injection slot shown in Fig. 1.

The light source for bubble illumination consisted of a 300-W quartz arc lamp, a rectangular aperture, and a 300-mm lens. The light source was located upstream and to one side of the tunnel and projected a beam through the tunnel wall into the cascade. The image of the aperture was focused in the cascade, and its vertical location was adjustable to illuminate either the boundary layer or the free stream. When viewed from above, or from the side, the bubbles showed up very brightly when they were in the light beam. Photographs of the bubbles were taken from two locations, directly above the cascade, providing a plan view of the flow, and upstream of the cascade, looking through the tunnel sidewall into the cascade, providing an oblique view of the flow. At either location, a motion picture camera, running at 3 frames per second, was used to record the bubble traces. The motion picture camera was merely a convenient way to acquire the data. Since the time of flight of the bubbles through the field of view was much shorter than the open time of the shutter, each frame was an independent data record. The bubbles appear as streaklines on the film, and adjacent frames of the film can never show the same bubble. The movies were viewed one frame at a time, and 35-mm copies were made of the most interesting frames.

A second technique used to visualize the flow was to inject smoke into the stream through a probe. A smoke generator was constructed, similar to that described in (1), and used also in (5). The source of the smoke was a burning, oil-soaked cigar. A regulated air supply provided combustion air, and the smoke was carried through a trap to allow large oil droplets to settle out, then it was ducted to the test section. The same lighting and camera system was used for the smoke as was used for the bubbles. The smoke had the advantage that it could be precisely placed where desired, but the disadvantage was that it diffused, and

being a continuous source, tended to average out temporal variations in the flow. This means that local details of the horseshoe vortex cannot be observed with smoke, but it does a good job of delineating regions of the flow and showing gross fluid motions.

Perhaps the most spectacular flow visualization pictures resulted from use of the ink dot technique developed by Langston and Boyle (11). For this procedure, a regular array of ink dots was laid down on a sheet of drafting film, using a permanent ink marker pen. The sheet was then rubber-cemented to the endwall surface, and a uniform layer of synthetic wintergreen oil was sprayed on the film. Then the facility flow was started and continued until the oil had all been dragged downstream and/or evaporated. What remained on the sheet was the array of dots, with tails originating from each dot, pointing in the direction of the local wall shear stress.

Additionally, some endwall surface flow visualization data were taken by placing small drops of light mineral oil mixed with a yellow pigment on the surface and recording on movie film the flow of the oil drops when air flow was established in the cascade. Comparison of the distance moved by different drops over the same number of movie frames gave an indication of the difference in wall shear stress at different points.

The four flow visualization techniques used can be put into two general catagories. The bubble and smoke methods show the motion of fluid "particles", while the ink dot and oil drop techniques delimit shear stress directions at the wall.

RESULTS AND DISCUSSION

Aerodynamic qualification

The initial work done in the facility served to qualify the rig and define the flow conditions.

The cascade periodicity was set by adjusting the tailboards until the variation in exit pressure difference (total pressure minus static pressure) between passages was minimized. At the final setting of the tailboards with the cascade operating at an inlet Reynolds number based on true chord of about 2.75×10^5, there was a variation of less than ±1 percent in the exit pressure difference between the five passages.

The pressure distribution around one of the vanes was measured and the results are shown in figure 2 as the ratio of local velocity to inlet critical velocity versus fraction of axial chord. A comparison of these data with the results presented in (9) shows good agreement, indicating that the vane profile used for the flow visualization tests is correctly scaled from the vanes in (9).

The cascade inlet boundary layer profile was measured at a point 21.6 cm upstream of the vanes using a Pitot-static probe. Profiles were taken at two flow conditions at nominal inlet Reynolds numbers of 2.3×10^5 and 1.6×10^5. The profile data were reduced to nondimensional form and compared with the universal turbulent boundary layer profile. The good agreement observed indicated that a fully developed turbulent boundary layer existed upstream of the vanes. For the two flow conditions, boundary layer thicknesses were about 1.9 (0.75) and 2.2 cm (0.85 in) respectively. These values are comparable, when scaled, with the inlet boundary layer thicknesses reported in (9).

Free stream turbulence intensity was measured at the same location as the boundary layer profiles, for the same two inlet Reynolds numbers. The results were 0.031 and 0.037, respectively. This is roughly half the turbulence level reported in (9).

Flow Visualization

Over the range of operating conditions available for the cascade it was observed that the flow visualization results were essentially independent of inlet conditions. There was no noticeable difference in bubble traces between the highest and the lowest inlet Reynolds number cases. The same was true for the smoke and the ink dot traces. Thus, in the descriptions to follow, specific flow conditions will not be discussed, rather, the best visual data available will be used regardless of flow conditions.

The results of using smoke to visualize the flow are presented in Fig. 3. Fig. 3(a) is a plan view photograph of a grid on the cascade endwall. The grid squares are 2.54 cm (1.0 inch) on a side. Fig. 3(b) shows smoke put in along a free-stream stagnation line. In this case, the smoke is far enough from the wall to be out of the endwall boundary layer, and shows very little spreading. The straight line seen near the pressure surface is the edge of the shadow of the vane leading edge falling on the smoke. The smoke did actually extend all the way to the pressure surface. For this picture, the light beam was grazing the endwall surface and had a thickness of about 4.8 cm. The picture shows bright highlights where the beam illuminates the vane surfaces, near the leading edge and the last half of the pressure surface. The bright spots on the endwall surface are light reflections from oil and dust particles on the surface. Fig. 3(c) shows the smoke injected into the endwall boundary layer, but still off the wall. Here the path of the smoke spreads very widely and a large region is filled with smoke. In this case, the smoke has been caught in the horseshoe vortex system.

Fig. 4 shows photographs of bubbles streaking through the cascade in the endwall boundary layer. For these pictures, the light beam was grazing the endwall surface and had a thickness of about 1 cm. Parts (a) and (b) show a plan view of the cascade (refer to Fig. 3(a) for the endwall scale). The wavy paths shown are actually plan views of corkscrew-like paths followed by bubbles that are caught in the horseshoe vortex. The core of the horseshoe vortex on the pressure side leg moves across the passage as it moves downstream, and analysis of the films at the trailing edge plane shows the location of the vortex to be centered at about two-thirds of the way from pressure to suction sides of the passage. Part (c) is an oblique view looking into the cascade at an angle with the inlet in the foreground. The corkscrew-like path of a bubble in the horseshoe vortex is more clearly seen in this view. Note also the extent of the light beam where it strikes the vane surfaces. The height of the beam was about 1 cm.

The different regions of flow on the endwall were most sharply outlined by use of the ink dot technique. Fig. 5 shows typical results from using this method. The stagnation streamlines and three-dimensional separation lines are apparent and have been highlighted in the figure for clarity. A detailed description of the significance of these features has been presented by Langston et al (2). The stagnation streamline separates flow between the suction and the pressure sides of the vane. The three-dimensional separation line divides the flow field adjacent to the endwall into distinct three-dimensional flow zones. Upstream of the three-dimensional separation, endwall flow is channeled toward the vane suction surface. The horseshoe vortex

is located downstream of this line and endwall flow is from the pressure side toward the separation line, leaving the surface at that point. The result shown in Fig. 5 is a black-and-white print of the actual data. In the actual test, two different colors of ink were used, one color in regions upstream of the three-dimensional separations, and another color downstream. The separation of the two regions is dramatically illustrated in this manner. In Fig. 5, the heavy black line has been added to show the location of the three-dimensional separation line. From the results of Fig. 5 it is apparent that all of the fluid entering the cascade very close to the endwall ends up on the suction surface of the vane. However, the smoke and bubble pictures show that most of the inlet boundary layer fluid ends up on the downstream side of the three-dimensional separation and leaves the cascade in the vortex. Langston et al (2) noted this same effect when they put smoke in the upstream boundary layer. A full color view of this figure was given to Langston and Boyle and has been published by them in (11) to demonstrate an application of the ink dot method.

The endwall flow visualization traces in Fig. 5 show the direction of the local wall shear stresses, but do not include any information about the magnitude. An attempt was made to gain information about the relative magnitude of the wall shear stress at different points on the endwall by an analysis of the motion picture of the flow of oil drops on the surface. It was assumed that for a given time interval, the length of the path followed by a given oil drop is proportional to the local wall shear stress. A justification of this assumption is presented by Atraghji (14). A number of drops were compared over a fixed number of movie frames, and their relative path lengths tabulated. Contours of constant relative motion were then sketched by hand, and the result is shown in Fig. 6. The higher numbers on the contours correspond to regions of higher shear stress.

Heat Transfer Comparison

Fig. 7 shows measured Stanton number contours overlaid with flow visualization information for two of the runs reported by Hylton et al (9). For these runs the exit Mach number and inlet Reynolds number were in the range tested in the flow visualization cascade. Two prominent peaks in Stanton number stand out, one near the vane leading edge on the pressure side, and one downstream of the trailing edge. A smaller peak occurs near the vane suction side, at about one-fourth of the axial chord into the passage. A region of relatively low Stanton number covers a large part of the first half of the midpassage area.

The most obvious correlation between the flow visualization data and the Stanton number contours in Fig. 7 is in the leading edge region, on the pressure side. The large gradient in Stanton number, leading to a peak in that area, coincides with the region of most intense vortex action, as shown by the smoke in Fig. 3 and the bubble traces in Fig 4. The smaller peak in Stanton number, near the suction surface, coincides with the region where the three-dimensional separation line reaches the suction surface. It is in this area where the oil on the endwall ahead of the separation line was observed to begin to climb onto the suction surface of the vane.

The large peak in Stanton number seen downstream of the vane trailing edge does not appear to be directly related to any of the horseshoe vortex features shown by the bubble traces, but the endwall ink dot traces in Fig. 5 show a diverging flow pattern on the endwall in this region. This would indicate that there is a flow of fluid toward the endwall in the vane wake, resulting in a high heat transfer coefficient. Comparing the midchannel region upstream and downstream of the three-dimensional separation line in Fig. 5 with the Stanton number contours in Fig. 7 shows that this is a region of relatively uniform, low Stanton number. Interestingly, there is nothing obvious in the Stanton number data that correlates with the location of the separation line.

SUMMARY AND CONCLUSIONS

Various flow visualization techniques were used to define the secondary flows near the endwall in a large-scale turbine vane cascade. The cascade was scaled up by a factor of 1.9 from one used to generate endwall heat transfer data under a joint NASA-USAF contract. A comparison of the visualized flow patterns and the measured Stanton number distributions was made for cases where the inlet Reynolds number and exit Mach number were matched. Flows were visualized by using neutrally buoyant helium-filled soap bubbles, by using smoke from oil soaked cigars, and by a technique using permanent marker pen ink dots and synthetic wintergreen oil.

From this investigation it can be concluded that

1. The only obvious correlation between the horseshoe vortex and the endwall heat transfer is near the vane leading edge where a local peak in heat transfer occurs and the initial vortex rollup begins.
2. The three-dimensional separation line on the endwall does not correlate with any endwall heat transfer features.
3. The large peak in Stanton number seen downstream of the vanes is not related to the horseshoe vortex, but appears to be related to downflow in the vane wake.
4. The ink dot surface flow visualization technique correlates well with boundary layer flow visualized by means of neutrally buoyant bubbles.

REFERENCES

1 Herzig, H. Z., Hansen, A. G., and Costello, G. R., " A Visualization Study of Secondary Flows in Cascades", NACA Report 1163, 1953.
2 Langston, L. S., Nice, M. L., and Hooper, R. M., "Three-Dimensional Flow Within a Turbine Cascade Passage", ASME Journal of Engineering for Power, Vol. 99, No.1, Jan. 1977, pp 21-28.
3 Langston, L. S., "Crossflows in a Turbine Cascade Passage", ASME Journal of Engineering for Power, V102, n4, 1980, pp 866-874.
4 Marchal, Ph., and Sieverding, C. H., "Secondary Flows Within Turbomachinery Bladings", AGARD CP-214, Advisory Group for Aerospace Research and Development, Paris (France), 1977, Paper 11.
5 Gaugler, R. E., and Russell, L. M., "Flow Visualization Study of the Horseshoe Vortex in a Turbine Stator Cascade", NASA TP-1884, 1982.
6 Blair, M. F., "An Experimental Study of Heat Transfer and Film Cooling on Large-Scale Turbine Endwalls", ASME Journal of Heat Transfer, Nov. 1974, pp 524-529.
7 Graziani, R. A., Blair, M. F., Taylor, J. R., and Mayle, R. E., "An Experimental Study of Endwall and Airfoil Surface Heat Transfer in a Large Scale Turbine Blade Cascade", ASME Journal of Engineering for Power, V102, n2, 1980, pp 257-267.

8 Georgiou, D. P., Godard, M., and Richards, B. E., "Experimental Study of the Iso-Heat-Transfer-Rate Lines on the End-Wall of a Turbine Cascade", ASME Paper No. 79-GT-20, Mar. 1979.

9 Hylton, L. D., Mihelc, M. S., Turner, E. R., and York, R. E., "Experimental Investigation of Turbine Endwall Heat Transfer", AFWAL-TR-81-2077, 3 Volumes, 1981.

10 York, R. E., Hylton, L. D., and Mihelc, M. S., "An Experimental Investigation of Endwall Heat Transfer and Aerodynamics in a Linear Vane Cascade", Proposed for presentation , ASME Gas Turbine Conference, March 1983.

11 Langston, L. S., and Boyle, M. T., "A New Surface Streamline Flow Visualization Technique", Journal of Fluid Mechanics, V 125, December 1982, pp. 53-57.

12 Yuska, J. A., Diedrich, J. H., and Clough, N., "Lewis 9- by 15-Foot V/STOL Wind Tunnel", NASA TM X-2305, 1971.

13 Hale,R. W., Tan, P., Stowell, R. C., and Ordway, D. E., "Development of an Integrated System for Flow Visualization in Air Using Neutrally Buoyant Bubbles", SAI-RR 7107, SAGE ACTION, Inc., Ithaca, N. Y. December, 1971. (AD-756691)

14 Atraghji, E., "More Than Meets the Eye: The Oil Dot Technique", International Symposium on Flow Visualization, Bochum, September, 1980, pp 67-68.

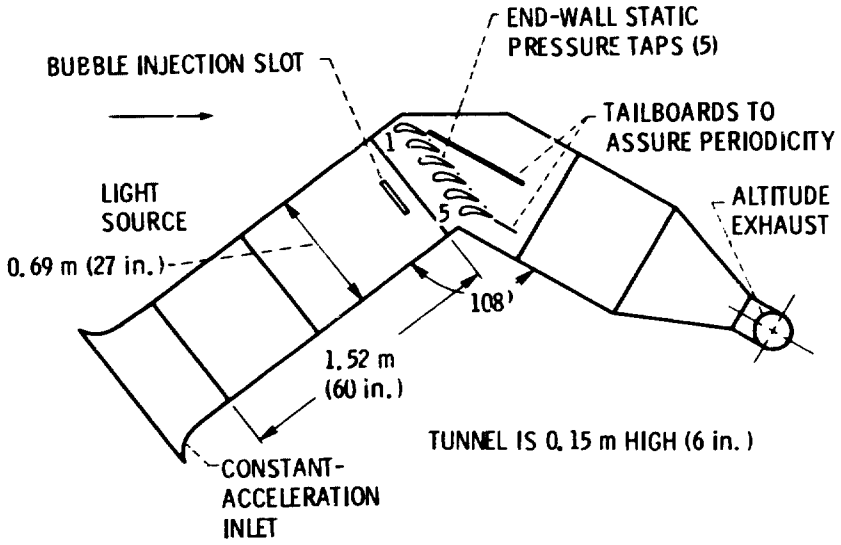

Figure 1. - Schematic plan view - flow visualization rig.

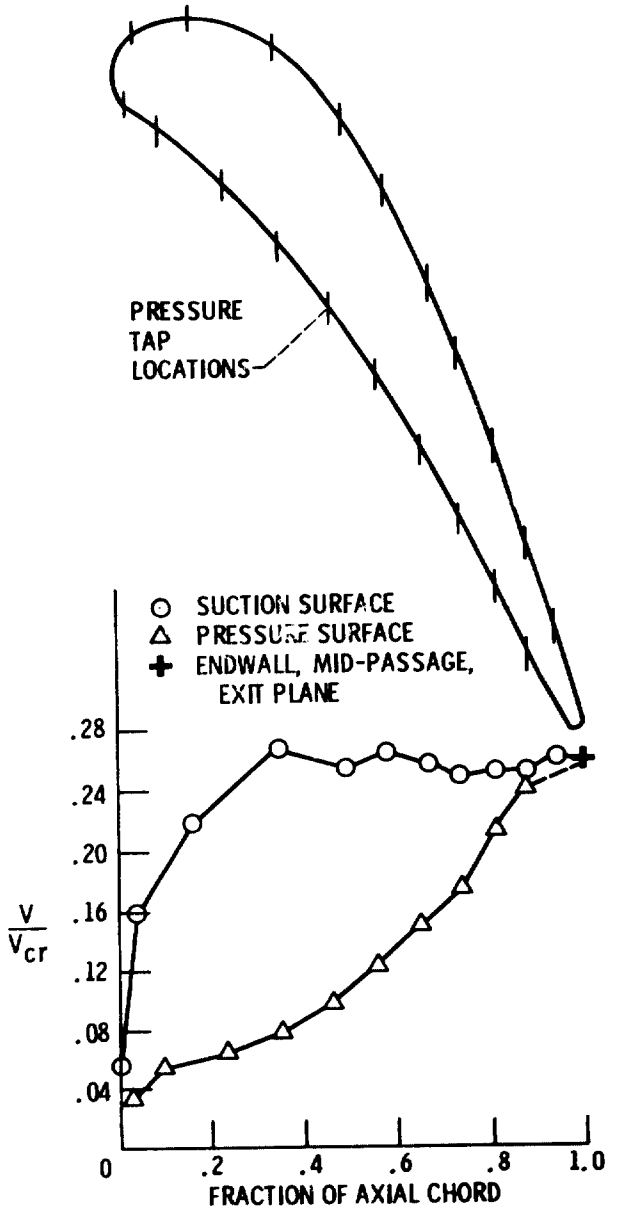

Figure 2. - Measured velocity distribution around the vane.

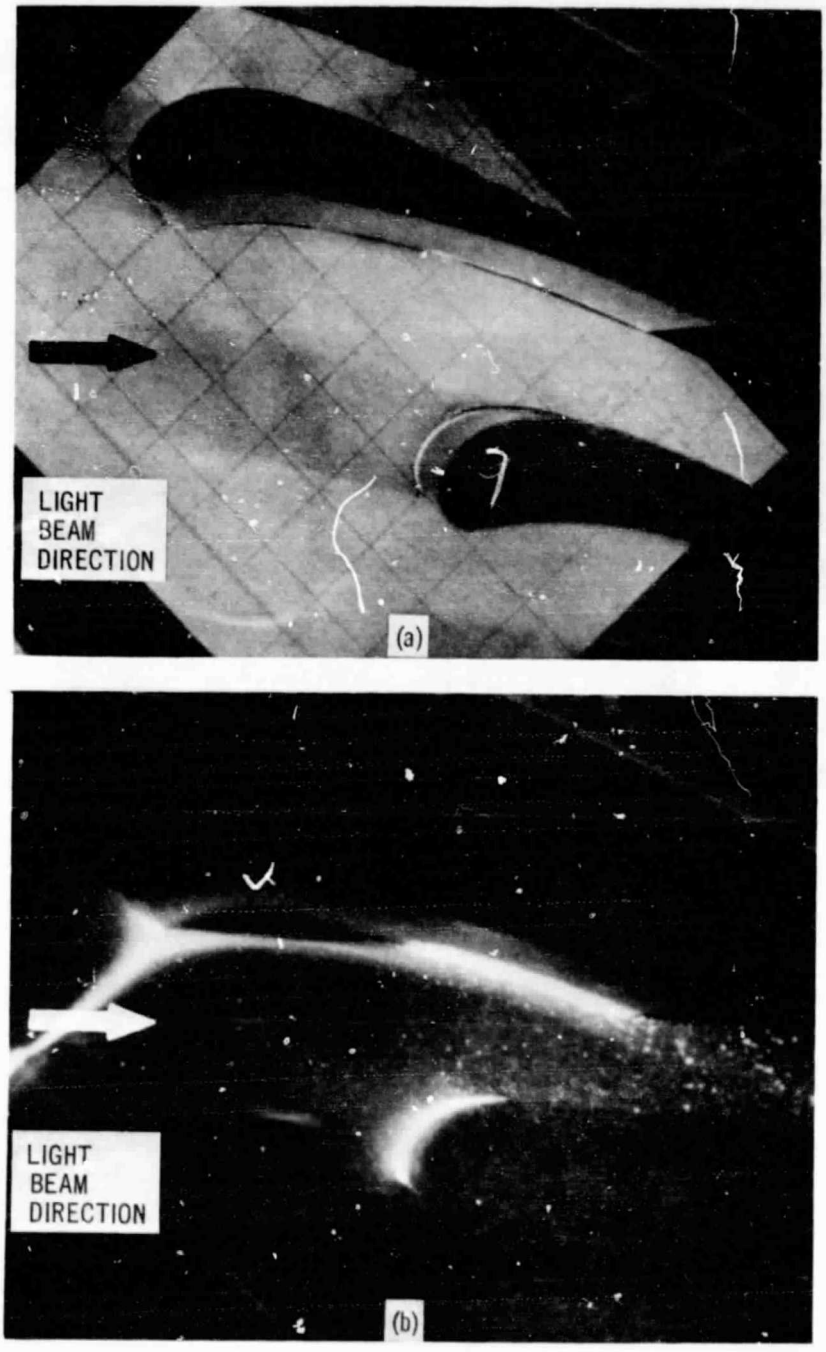

(a) Endwall scale, 2.54 cm (1 in) grid.

(b) Smoke on stagnation streamline, but in the free stream, out of the endwall boundary layer.

Figure 3. - Smoke flow visualization, plan view.

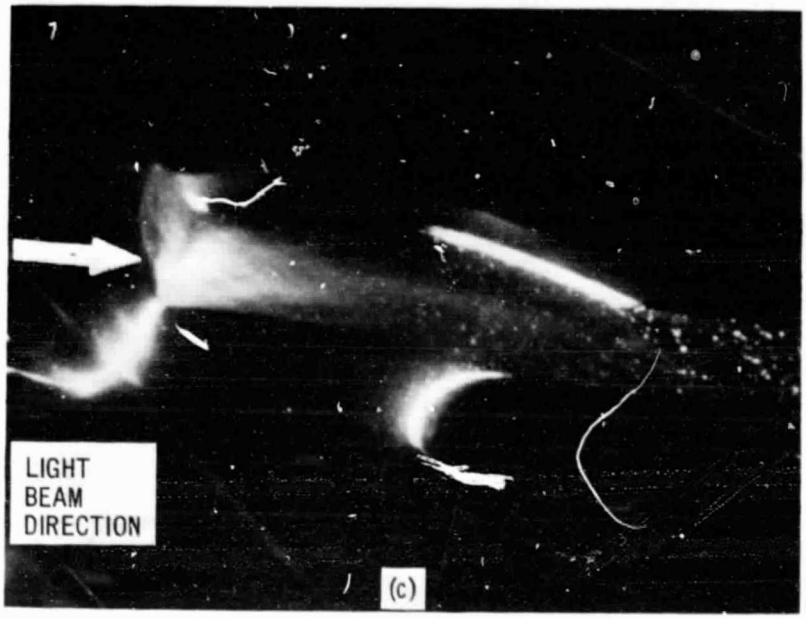

(c) Smoke on stagnation streamline, but in the outer part of the endwall boundary layer.

Figure 3. - Concluded.

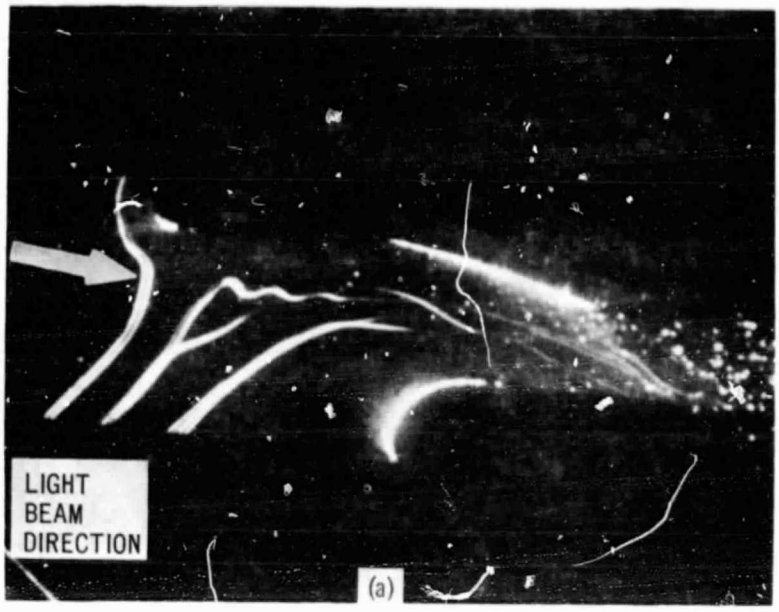

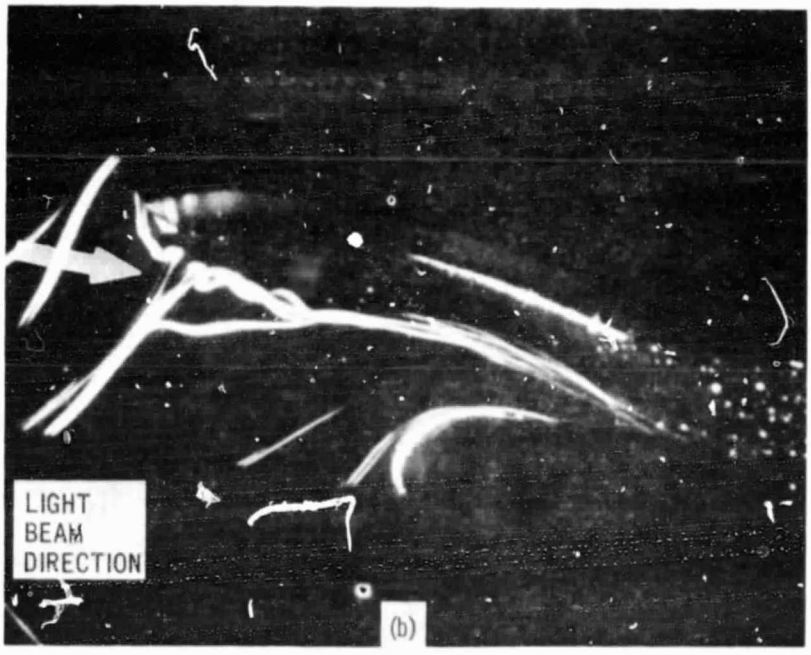

(a) Plan view.

(b) Plan view.

Figure 4. - Neutrally-buoyant, helium-filled, soap bubble traces in the endwall boundary layer.

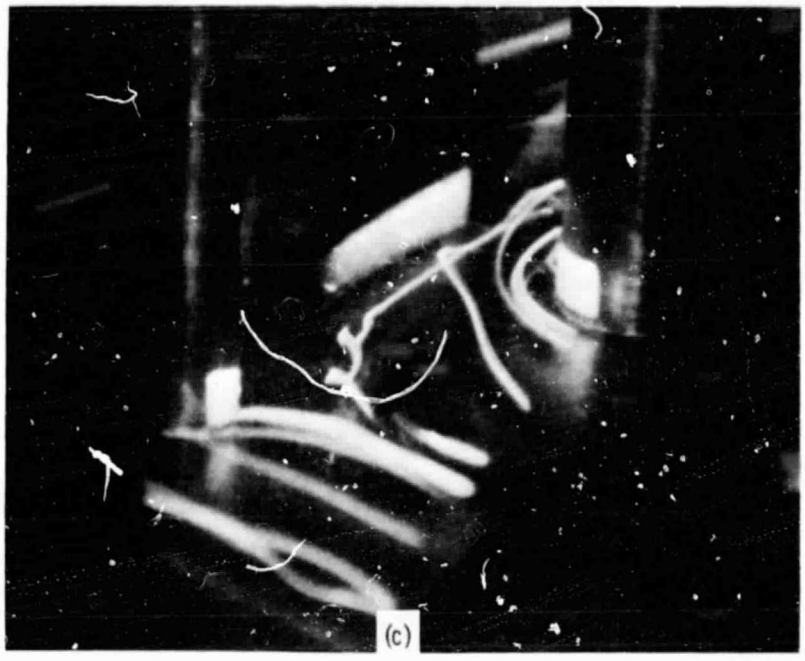

(c) Oblique view.

Figure 4. - Concluded.

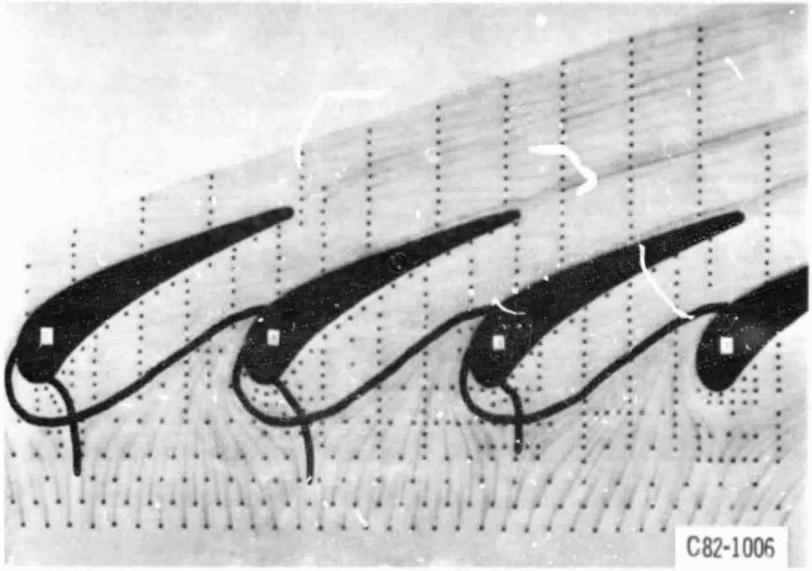

Figure 5. - Ink dot flow visualization of the endwall surface secondary flows. Solid lines illustrate the location of the three-dimensional separation line and stagnation streamline.

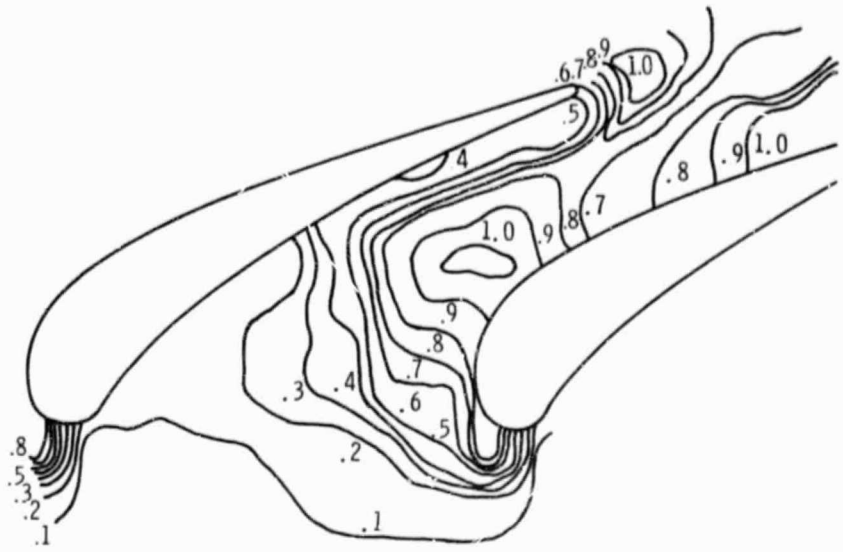

Figure 6. - Endwall contours of lines of constant non-dimensional wall shear stress.

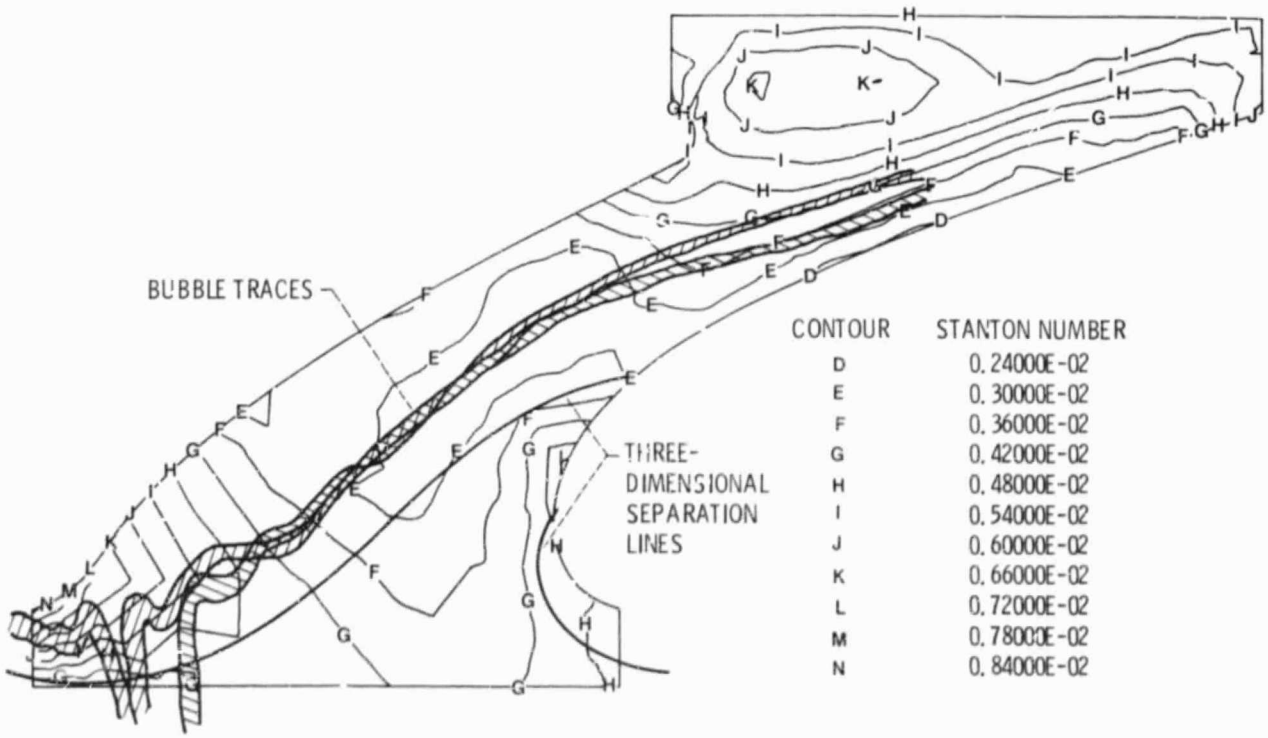

(a) Run 124, inlet Reynolds number = 0.208×10^6 (reference 9).

Figure 7. - Comparison of endwall Stanton number contours and visualized secondary flows.

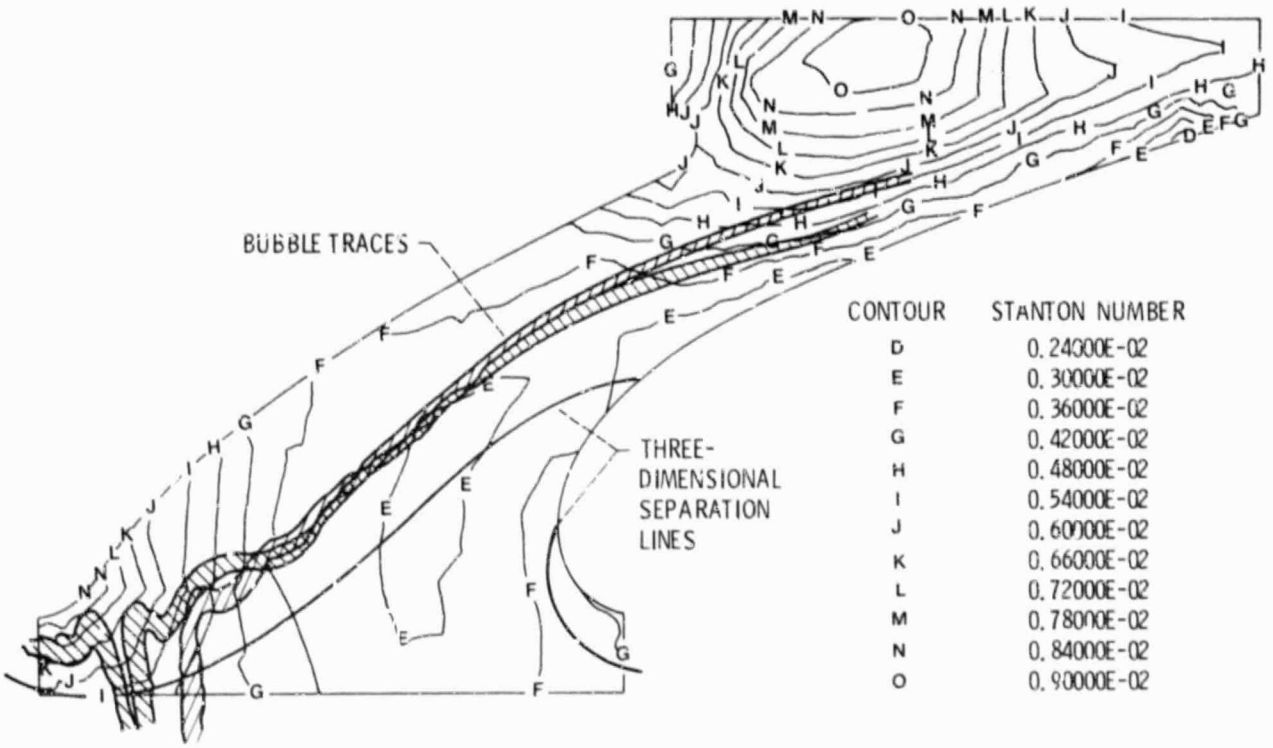

(b) Run 131, inlet Reynolds number = 0.296×10^6 (reference 9).

Figure 7. - Concluded.